Chapter VI

Adsorption using Treated Vicia faba husks (TVFH)

Chapter VI

Adsorption using Treated *Vicia faba* Husks (TVFH)

Deliberations regarding the applicability of treated *Vicia faba* husk (TVFH) in trapping PO_4^{3-}, NO_3^- and SO_4^{2-} anions from aqueous matrices are as follows:

6.1 Microscopic Analysis

The microscopic views of 85 BSS mesh size (raw/ treated) VFH are depicted in fig 6.1a & 6.1b.

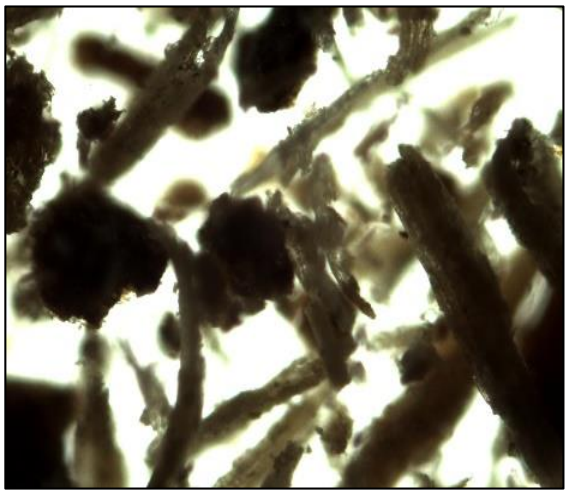

Figure 6.1a Raw VFH

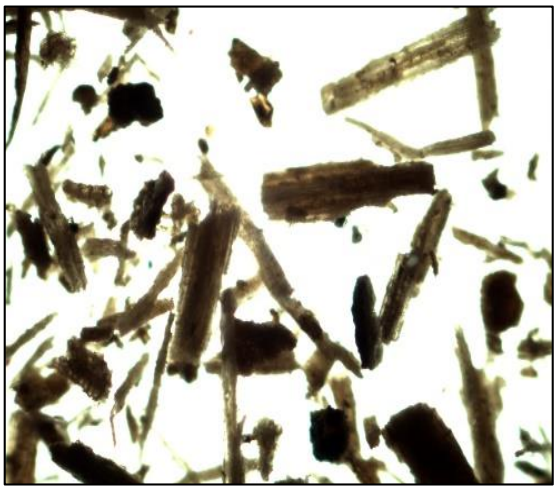

Figure 6.1b Treated VFH

6.2 Physio- Chemical Characterization

Physio-chemical properties of TVFH (0.18mm) is listed in table 6.1. Low values for the parameters, viz., bulk density, specific gravity, moisture/ash contents, acid/ water soluble matter for TVFH resemble that of TCSS, thenceforth favour sorption process. This is supported by pH_{zpc} value, promoting anions sorption onto the outer surface[1]. Among the analysed elements/ groups, greater percentage of carbon content and carboxylic nature reveal the sorption capacity of material due to electrostatic interaction property.

Table 6.1 Physio- Chemical Characteristics

Properties	TVFH (0.18 mm)
pH	6.13
Conductivity(mV)	32.24
Moisture (%)	1.38
Bulk density (g/L)	0.62
Specific gravity	1.08
Porosity	50.19
Ash content (%)	3.89
Acid Soluble Matter (%)	1.96
Water Soluble Matter (%)	1.14
Ion Exchange Capacity (meq /g)	0.54
pHzpc	6.11
Surface area (m^2/g)	31.42
Mean Pore diameter (nm)	5.0
Carbon (%)	44.68
Nitrogen (%)	1.79
Hydrogen (%)	6.25
Sulphur (%)	0.42
Surface Acidic groups (m mol g^{-1})	
Phenolic	0.68
Carboxylic	1.63
Lactonic	0.17

Surface area (31.42 m^2/g) and internal pore values (5 nm) were derived from BET/ BJH techniques, registering the mesoporous nature of TVFH material. Meagre broad H_3 type hysteresis loop (clear hysteresis at $P/P° > 0.6$) represents the aggregates of slit – like pores[2] (fig 6.2).

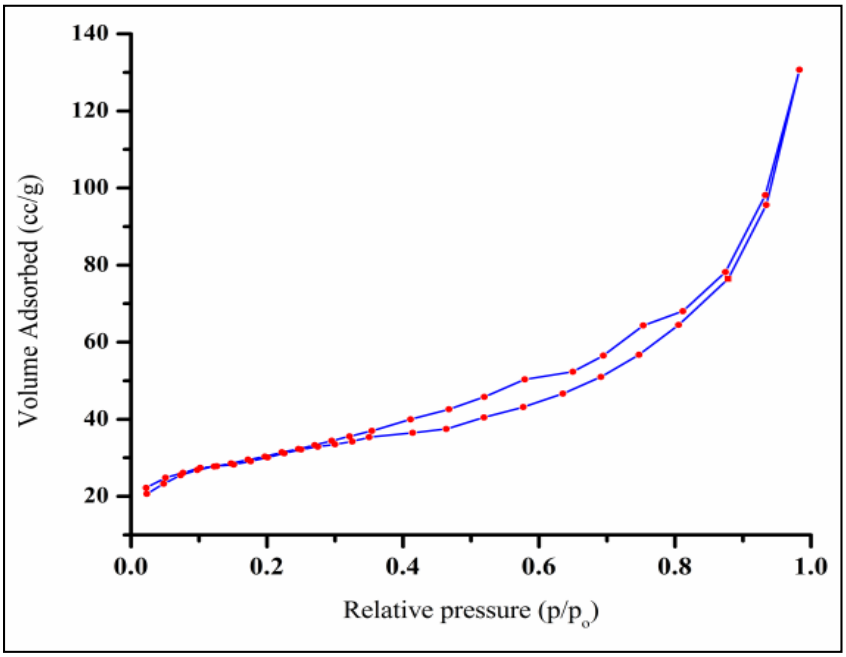

Figure 6.2 Adsorption / Desorption Isothermal Plot

6.3 SEM and EDAX Analyses

In SEM micrograph, raw material (fig 6.3) shows flake like form of the *faba* husk, with the irregular surface, full of protrusions and cracks. In case of unloaded material, chemical modification has degraded lignin and spaced out the fibrils (fig 6.4). Loaded counterparts (figs 6.5 – 6.7) exhibit multilayer structure on surface, proving the enhancement in anion binding morphology[3].

Appearance of new specific anion peaks at a value of 1 - 3 KeV confirms the sequestration of specific anions as depicted in EDAX spectra (figs 6.9 – 6.11), against unloaded spectra. (fig 6.8)

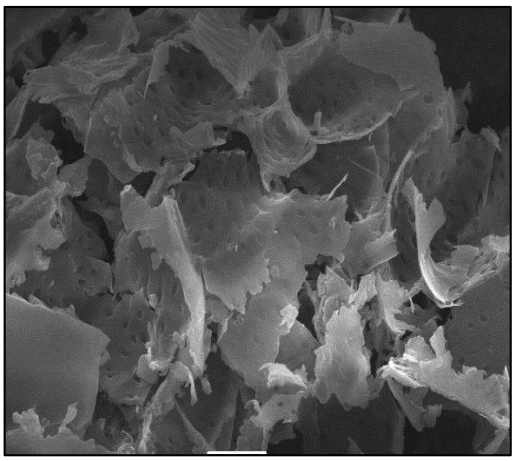

Figure 6.3 Raw VFH

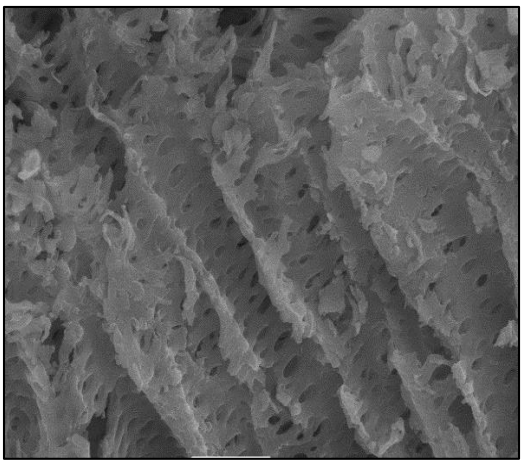

Figure 6.4 Unloaded TVFH

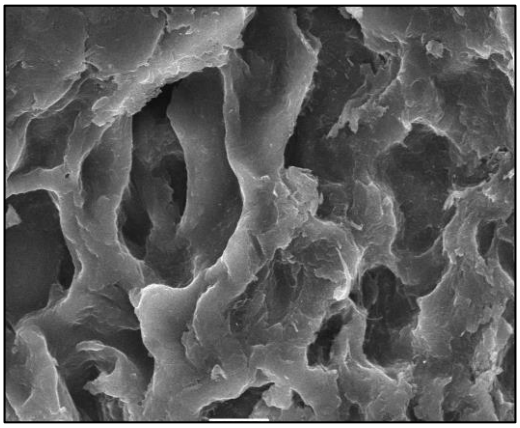

Figure 6.5 PO_4^{3-} loaded TVFH

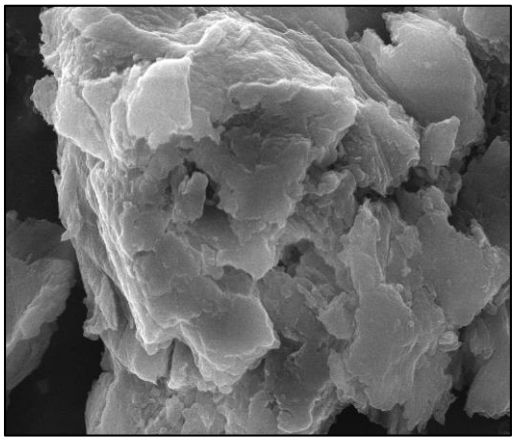

Figure 6.6 NO_3^- - loaded TVFH

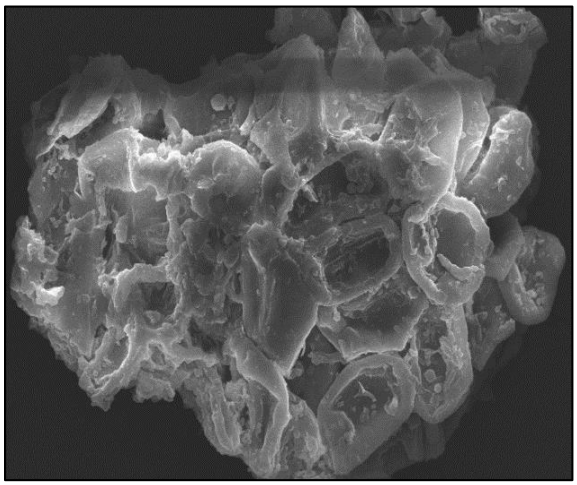

Figure 6.7 SO_4^{2-} - loaded TVFH

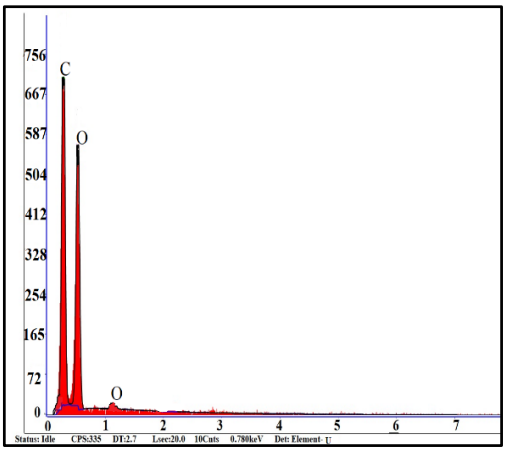

Figure 6.8 Unloaded TVFH

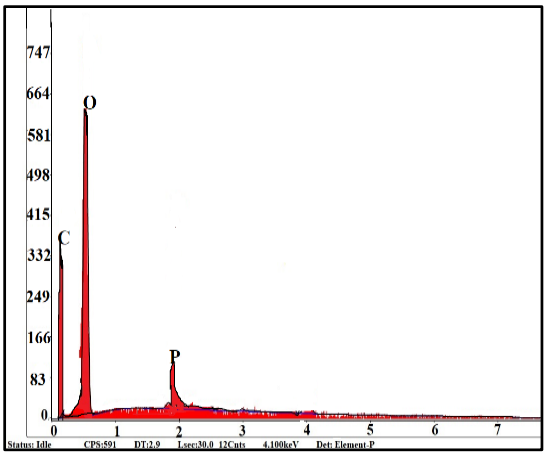

Figure 6.9 PO_4^{3-} loaded TVFH

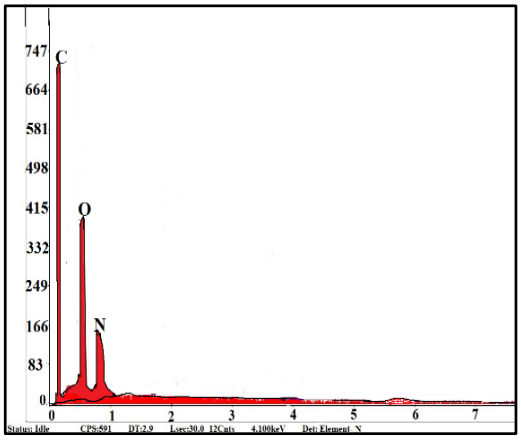

Figure 6.10 NO_3^- loaded TVFH

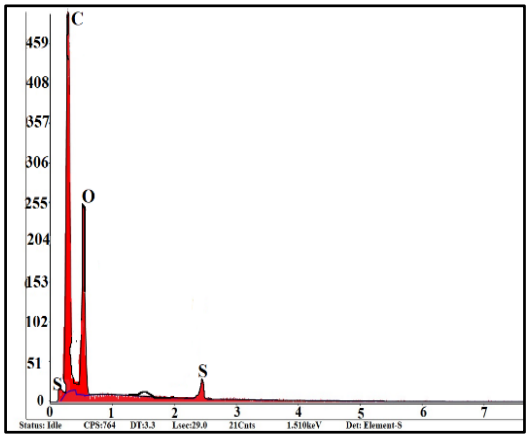

Figure 6.11 SO_4^{2-} loaded TVFH

6.4 FT-IR Spectral Studies

FT-IR spectra of TVFH system is shown in figure 6.12. A strong bands at 3745.85cm^{-1} and 2930.20 cm^{-1} indicate stretching vibrations of -OH, -NH_2 and C-H groups. The prominent peak 1638.21cm^{-1} imply a bending vibration of -C=N- bond, which may be characteristic of the sorbate-sorbent interaction. Characteristic vibrations with reference to anion-oxygen stretching is inferred from the bands at 1038.11 cm^{-1} and 662.22 cm^{-1}. Participation of these functional groups in the binding process of anions onto the TVFH surface is confirmed by the variations in peak intensities and appropriate shifts in the bands.

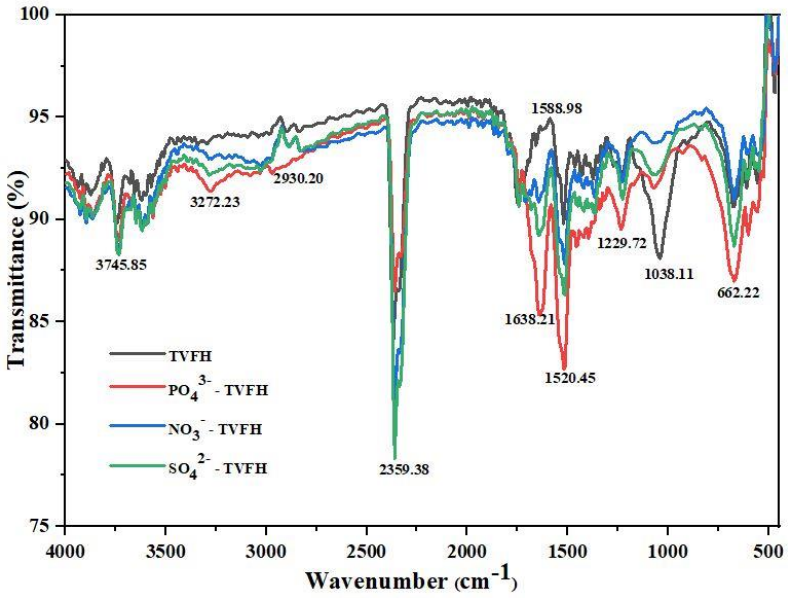

Figure 6.12 FTIR Spectra

6.5 Batch Equilibration Studies

6.5.1 Impact of Particle Size

Figure 6.13 displays the amounts of anions adsorbed by varying particle sizes of TVFH. The graphical trend is similar to those discussed in previous two chapters, thereby leading to fixation of 0.18 mm particle size for further experiments.

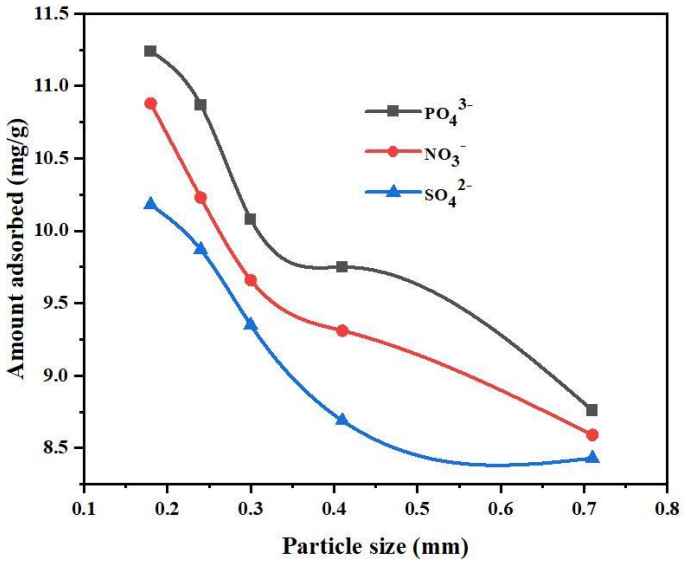

Figure 6.13 Impact of Particle size

6.5.2 Impact of Initial Concentration and Agitation Time

The amount of anions adsorbed by TVFH at varying initial anion concentrations/ time frames are tabulated in table 6.2. The initial concentrations for the studied anions were fixed for TVFH, as that of TETS systems, which is proclaimed from the listed values. However, rapid uptake of anions had occurred maximum, initially upto 10 minutes against that of 5 minutes, as reported in earlier chapter.[6]

Table 6.2 Impact of Initial Concentration and Agitation Time

System	Time (min)	Amount Adsorbed (mg/g)					
		50 mg/L	100 mg/L	150 mg/L	200 mg/L	250 mg/L	300 mg/L
PO_4^{3-} - TVFH	5	32.24	43.16	40.86	38.90	35.82	32.32
	10	38.81	**46.54**	41.82	40.65	38.08	37.72
	15	33.54	44.25	40.64	40.13	36.65	35.26
	20	30.62	42.16	39.44	39.32	35.33	34.82
	25	27.92	41.40	38.56	38.56	34.84	32.67
	30	25.54	40.49	37.32	36.15	32.54	30.58
NO_3^- - TVFH	5	24.11	36.42	32.92	30.68	30.13	29.94
	10	26.58	**40.17**	36.65	33.21	32.32	31.53
	15	25.72	39.18	34.18	32.53	31.61	30.48
	20	24.98	38.15	32.84	31.23	31.28	30.23
	25	23.62	37.53	32.26	31.06	30.94	29.94
	30	21.14	36.49	31.14	30.72	29.86	29.09
SO_4^{2-} - TVFH	5	24.93	27.13	30.86	35.84	39.81	32.79
	10	27.56	30.48	34.92	37.49	**44.95**	36.93
	15	25.94	28.95	33.49	36.84	42.41	34.75
	20	23.75	27.21	32.14	35.49	40.61	31.14
	25	22.32	26.58	30.68	34.08	38.13	30.85
	30	20.94	25.46	31.39	32.51	36.69	29.72

6.5.3 Impact of TVFH Dosage

Table 6.3 records approximately 93 % removal for PO_4^{3-} , NO_3^- / SO_4^{2-} ions at respective doses of 200/ 250 mg. Further increase in dosage may lead to the overcrowding of sorbent particles, making themselves available for chelation of sorbate species, referred to as solid concentration effect[7].

Table 6.3 Impact of Dosage

Anions	Percentage Removal (%)					
	50 mg	**100 mg**	**150 mg**	**200 mg**	**250 mg**	**300 mg**
PO_4^{3-}	80.3	85.4	89.6	**93.8**	90.2	89.7
NO_3^-	72.5	83.8	87.3	**92.6**	88.8	87.4
SO_4^{2-}	74.6	80.4	86.6	89.2	**92.9**	88.3

6.5.4 Impact of pH

Systematic inverted parabolic curves[8] representing maximum anion sorption at pH 5 is evident from figure 6.14. The diminshed sorption rate at alkaline pH ranges may be due to electrostatic repulsion between anionic sites.

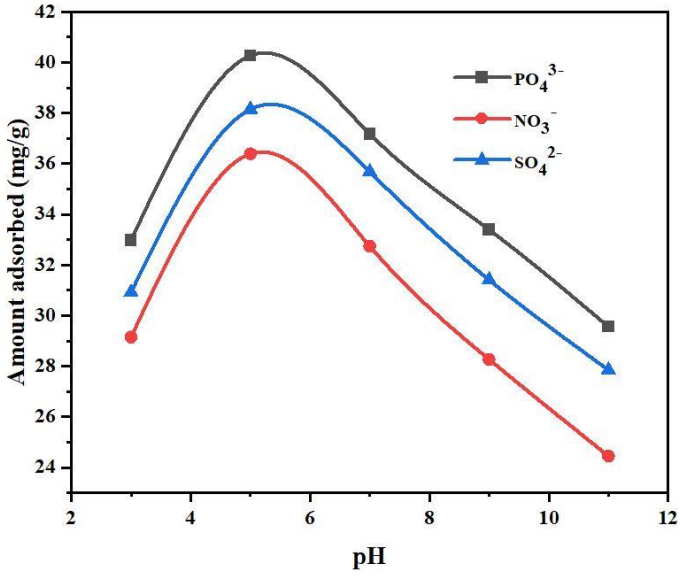

Figure 6.14 Impact of pH

6.5.5 Impact of Ions

Cationic/co-ionic influence upon TVFH systems at specific concentrations recorded apparent inhibition by magnesium ions[9] as listed in table 6.4. It has been reported that multivalent anions with higher charge density adsorb more readily than monovalent coions[10].

Table 6.4 Impact of Ions

Systems	Anion removal in absence of ions	Conc. (mg/L)	Percentage removal (%)			
			Cations		Co ions	
			Mg^{2+}	Na^{+}	Cl^{-}	F^{-}
PO_4^{3-} -TVFH	93.8	100	**74.3**	76.6	83.9	85.6
		200	73.7	75.4	82.7	84.3
		300	72.6	74.9	81.6	83.4
		400	71.4	73.8	80.5	82.5
		500	70.6	71.9	79.3	81.1
NO_3^{-} -TVFH	92.6	100	**66.8**	69.8	80.7	82.6
		200	65.9	68.7	79.4	81.9
		300	64.5	67.6	79.1	81.3
		400	63.7	66.3	78.7	80.8
		500	62.4	65.2	77.2	79.5
SO_4^{2-} -TVFH	92.9	100	**71.7**	74.9	81.8	84.2
		200	70.5	73.3	80.6	83.8
		300	69.6	72.5	79.4	82.7
		400	68.8	71.7	78.5	81.5
		500	68.3	70.6	77.8	80.4

6.5.6 Impact of Temperature

Inclined sorption capacities are registered with temperatures, indicative of greater penetration of anions[11] into mesoporous TVFH. The above statement is reflected upon the values in table 6.5.

Table 6.5 Impact of Temperature

System	Amount adsorbed (mg/g)				
	293 K	**303 K**	**313 K**	**323 K**	**333 K**
PO_4^{3-} - TVFH	46.54	49.8	56.6	59.9	65.7
NO_3^-- TVFH	40.17	43.2	45.3	49.6	57.5
SO_4^{2-} - TVFH	44.95	46.6	53.9	57.2	62.4

6.5.7 Desorption/ Regeneration Studies

Desorption/regeneration concentrate on the probability of sorbent recycling and sorbate reclamation. Observance of adsorbate species on the adsorbent surface can either be through physical bonding/ ion exchange or a combination of both. Experimental setup for the aforesaid studies were identical to those describe in former chapters, wherein 0.01N strength is fixed for HCl eluent and degradation in regeneration efficiency was observed for subsequent desorption cycles.

6.5.8 Statistical Analysis

The calculated positive/ negative Pearson correlation values (table 6.6) are observed as $P < 0.05$, justifying the experimental results.

Table 6.6 Statistical Data

System	Parameter	Descriptive			Pearson Correlation	P	ANOVA	
		Mean	SD	SE			F	F_{crit}
PO_4^{3-} - TVFH	Particle size	11.72	0.35	0.78	-0.9275	$6.66E^{-06}$	976.29	5.31
	Initial anion concentration	41.54	2.09	0.85	0.4047	0.0065	12.20	4.96
	Dosage	42.02	4.51	1.84	0.4548	0.0081	12.09	4.96
	pH	41.54	2.09	1.85	-0.8062	0.0003	103.30	5.31
NO_3 - TVFH	Particle size	10.99	0.39	0.28	-0.9960	$4.63E^{-06}$	1279.58	5.31
	Initial anion concentration	33.54	4.08	1.66	0.4047	0.0065	13.69	4.96
	Dosage	38.12	4.18	1.70	0.4546	0.0081	12.82	4.96
	pH	35.54	4.08	1.66	-0.8887	0.0008	162.54	5.31
SO_4^{2-} - TVFH	Particle size	9.62	0.64	0.28	-0.9744	$8.37E^{-06}$	937.06	5.31
	Initial anion concentration	31.88	4.74	1.93	0.4257	0.0061	14.00	4.96
	Dosage	41.18	4.06	1.66	0.7782	0.0075	12.25	4.96
	pH	31.88	4.74	1.93	-0.8898	0.0004	148.74	5.31

6.6 Adsorption Isotherms

Four empirical models viz., Langmuir, Freundlich, Temkin and DKR isotherms were applied to the sorption systems of TVFH. These isotherms relate anion uptake per unit weight of the adsorbent q_e against the equilibrium anion concentration in the bulk phase C_e. Calculated equilibrium concentrations and constant values are listed in tables 6.7 and 6.8.

Table 6.7 Equilibrium Concentrations- Isothermal Study

System	Anion Conc. (mg/L)	Langmuir		Freundlich		Temkin		DKR	
		C_e	C_e/q_e	log C_e	log q_e	ln C_e	q_e	ε^2*10^{-5}	ln q_e
PO_4^{3-} TVFH	50	9.83	0.67	1.03	1.20	2.38	9.81	0.49	2.77
	100	14.94	0.67	1.07	1.31	2.47	11.23	0.41	3.02
	150	33.64	0.74	1.31	1.50	3.02	12.32	0.14	3.46
	200	64.36	0.81	1.56	1.55	3.59	13.65	0.04	3.57
	250	89.14	0.89	1.69	1.70	3.89	14.83	0.02	3.92
	300	128.42	0.94	1.76	1.77	4.06	17.82	0.01	4.09
NO_3^--TVFH	50	14.18	0.73	1.15	1.28	2.65	12.82	0.29	2.95
	100	18.13	0.75	1.30	1.35	3.00	13.68	0.14	3.12
	150	31.84	0.77	1.47	1.58	3.39	14.32	0.06	3.64
	200	65.86	0.82	1.73	1.81	3.98	14.97	0.02	4.17
	250	94.63	0.88	1.92	1.98	4.43	15.64	0.01	4.56
	300	143.24	0.92	2.00	2.03	4.61	16.23	0.01	4.69
SO_4^{2-} TVFH	50	17.24	0.76	1.18	1.29	2.72	9.48	0.25	2.96
	100	22.63	0.79	1.35	1.45	3.11	10.32	0.11	3.30
	150	43.58	0.83	1.63	1.71	3.77	12.48	0.03	3.96
	200	57.67	0.85	1.74	1.81	4.01	13.67	0.02	4.15
	250	88.53	0.92	1.94	1.98	4.48	13.94	0.01	4.56
	300	132.16	0.95	2.03	2.05	4.69	15.89	0.01	4.73

Table 6.8 Isothermal Constants

System	Langmuir			Freundlich			Temkin			DKR		
	q_m (mg/g)	B	R^2	K_F (mg/g)	1/n	R^2	A_T (L/g)	B_T (J/mol)	R^2	q_s (mg/g)	E (KJ/mol)	R^2
PO_4^{3-} - TVFH	**52.2**	0.09	0.9973	3.44	0.28	0.9315	8.08	95.66	0.8915	49.90	4.66	0.9552
NO_3^- - TVFH	**45.19**	0.02	0.9966	1.59	0.57	0.9028	5.81	53.51	0.8748	80.55	1.09	0.9428
SO_4^{2-} - TVFH	**46.53**	0.02	0.9942	1.76	0.46	0.9163	6.12	77.38	0.8866	82.75	2.93	0.9593

6.6.1 Langmuir Model

Langmuir constants, viz., adsorption capacity (q_m) and energy of adsorption (b) derived from the plot C_e/q_e vs C_e (fig 6.15) favour monolayer sorption. Also, the dimensionless equilibrium factor (R_L) calculated as per equation 12, ranges between 0 to 1 describing beneficial adsorption[12]. Predominate lying of points in the linear form shows their R^2 values to be around unity value.

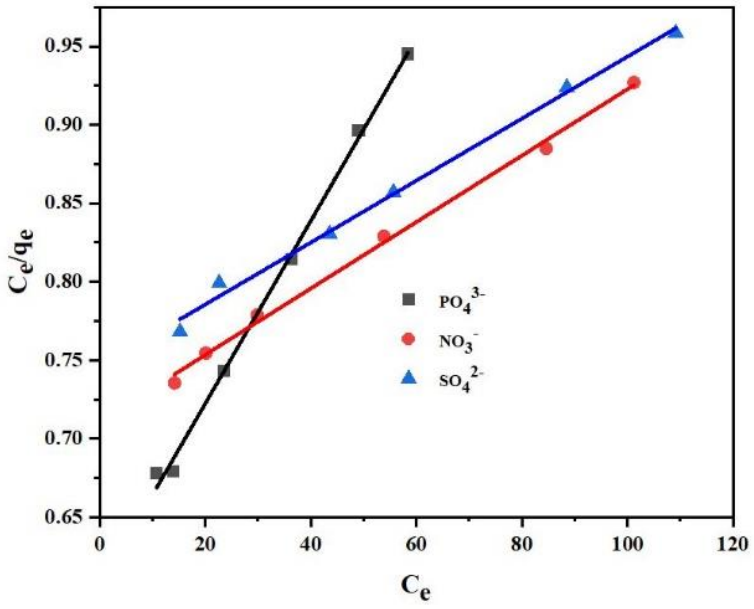

Figure 6.15 Langmuir Plot

6.6.2 Freundlich Model

Freundlich expression encompasses the surface heterogeneity and the exponential distribution of TVFH active sites and their energies. Sorption intensity (1/n) values, exponentially lie in the range lower than unity, indicating less applicability of the model[13].

6.6.3 Temkin Isotherm Model

Temkin model enables the determination of the constants A_T (binding energy) and b_T (heat of sorption) as given in the table 6.8. Lower A_T and higher b_T values imply minimal suitability of this model.[14]

6.6.4 Dubinin– Kaganer- Radushkevich (DKR) Isotherm

DKR constants q_s (saturation sorption capacity) and E (mean free energy) were calculated similarly as done in previous chapters, wherein, values of E lesser than 8 KJ/mol specify the predominance of physisorption[15].

6.6.5 Comparison of Isotherm Models

The order of best suitability of applied isothermal models to TVFH systems is sufficed with obtained isothermal constants and correlation coefficient values, shown as: Langmuir > DKR > Freundlich > Temkin.

6.7 Adsorption Kinetics

Understanding the adsorption mechanism and potential rate controlling steps such as chemical reaction, diffusion control and mass transport processes is made possible through the examination of kinetic models. The experimental data were tested with kinetic equations to determine the adsorption reactions.

6.7.1 Pseudo First Order/ Pseudo Second Order Models

Table 6.9 exhibits the calculated data for pseudo-first/ second -order kinetic models at optimized concentrations. Kinetic rate constants, R^2/ SSE values were recorded from respective graphs as in previous chapters, being represented in table 6.10. From R^2 values, it is observed that description about the adsorption of anions is more pronounced for Pseudo second order model.

Table 6.9 Pseudo Models – Data

Time (min)	PO_4^{3-} - TVFH			NO_3^--TVFH			SO_4^{2-} - TVFH		
	log (qe-qt)	qt	t/qt	log (qe-qt)	qt	t/qt	log (qe-qt)	qt	t/qt
5	1.82	33.32	0.15	1.87	25.74	0.19	1.84	29.88	0.16
10	1.82	32.68	0.30	1.87	24.46	0.40	1.84	29.23	0.34
15	1.83	31.53	0.47	1.88	23.83	0.62	1.85	28.46	0.52
20	1.83	30.92	0.64	1.88	22.59	0.88	1.86	27.18	0.73
25	1.84	30.26	0.82	1.89	21.37	1.16	1.86	26.56	0.94
30	1.84	29.45	1.01	1.89	20.62	1.45	1.87	25.67	1.16

Table 6.10 Pseudo First Order/ Pseudo Second Order Parametric values

Conc. of Anions (mg/L)	$q_{exp.}$ (mg/g)	Pseudo First Order				Pseudo Second Order			
		$q_{cal.}$ (mg/g)	$K_1\times10^{-3}$ (min^{-1})	R^2	SSE	$q_{cal.}$ (mg/g)	$K_2\times10^{-3}$ (min^{-1})	R^2	SSE
PO_4^{3-} - TVFH									
50	38.81	19.24	0.01	0.9371	9.78	39.21	0.01	0.9979	0.02
100	**56.54**	71.07	0.02	0.9534	39.97	**48.81**	0.03	0.9989	3.86
150	42.82	122.77	0.01	0.9318	59.97	36.80	0.02	0.9988	3.01
200	41.65	175	0.06	0.9153	87.13	38.24	0.05	0.9999	1.70
250	41.64	228.92	0.04	0.9201	93.64	37.06	0.02	0.9979	2.29
300	40.26	284.64	0.06	0.9244	121.19	33.14	0.04	0.9944	3.56
NO_3^- - TVFH									
50	26.72	45.94	0.09	0.9473	9.61	31.94	0.01	0.9979	2.37
100	**46.07**	80.70	0.02	0.9589	20.76	**41.93**	0.02	0.9996	4.19
150	35.18	131.09	0.01	0.9429	47.95	33.80	0.02	0.9978	0.69
200	34.53	184.03	0.06	0.9321	74.75	30.79	0.26	0.9962	1.87
250	33.61	239.27	0.09	0.9465	102.83	28.03	0.13	0.9987	2.79
300	32.48	294.30	0.06	0.9312	130.91	27.57	0.09	0.9982	2.58

Conc. of Anions (mg/L)	$q_{exp.}$ (mg/g)	Pseudo First Order				Pseudo Second Order			
		$q_{cal.}$ (mg/g)	$K_1 \times 10^{-3}$ (min^{-1})	R^2	SSE	$q_{cal.}$ (mg/g)	$K_2 \times 10^{-3}$ (min^{-1})	R^2	SSE
SO_4^{2-} - TVFH									
50	29.94	70.05	0.01	0.9393	14.94	36.36	0.01	0.9978	3.21
100	33.41	171.41	0.06	0.9243	69.00	26.95	0.04	0.9982	3.23
150	34.84	169.24	0.18	0.9551	67.20	34.93	0.07	0.9985	0.04
200	35.24	170.05	0.15	0.9359	67.40	36.36	0.19	0.9978	0.56
250	**48.34**	175.52	0.02	0.9598	69.51	**46.39**	0.02	0.9979	1.22
300	34.73	160.41	0.06	0.9423	62.84	30.95	0.16	0.9992	1.55

6.7.2 Elovich Model

Notable β values at higher concentrations is evident from the derived Elovich constants, as mentioned in table 6.11, the reason for which may be the availability of excess anion species, covering the surface extensively, in turn rising the activation energy of the studied systems[16].

Table 6.11 Elovich Constants

Conc. (mg/L)	PO_4^{3-} - TVFH			NO_3^--TVFH			SO_4^{2-} - TVFH		
	α	β	R^2	α	β	R^2	α	β	R^2
50	26.86	1.72	0.9396	20.04	1.44	0.9586	23.93	1.60	0.9755
100	25.65	1.81	0.9140	15.50	1.68	0.9217	18.34	1.75	0.9508
150	24.47	1.92	0.9527	16.21	1.73	0.9338	17.35	1.87	0.8973
200	21.32	2.34	0.9669	13.27	1.87	0.9109	15.28	2.16	0.9078
250	18.68	2.72	0.8915	7.15	2.05	0.8973	11.41	2.37	0.9307
300	11.18	2.89	0.9515	2.64	2.46	0.8855	9.52	2.53	0.9561

6.7.3 Intraparticle Diffusion Model

K_{id} and C values (table 6.12), is noticed to be directly proportional to anion concentrations. This shows that a resistance may be developed at the boundary layer of diminished thickness, with reference to the transfer of sorbate mass[17].

Table 6.12 Intraparticle Diffusion Constants

Conc. (mg/L)	PO_4^{3-} - TVFH		NO_3^--TVFH		SO_4^{2-} - TVFH	
	K_{id}	C	K_{id}	C	K_{id}	C
50	1.71	15.15	1.05	11.34	1.49	13.83
100	1.99	19.37	1.59	16.68	1.71	17.83
150	2.07	22.32	1.75	19.38	1.90	20.35
200	2.52	25.25	2.04	23.11	2.34	24.60
250	2.98	29.37	2.45	27.19	2.63	28.42
300	3.62	32.45	2.51	29.10	3.57	30.76

6.7.4 Comparison of Kinetic Models

Experimental data exposed better compliance with the pseudo-second-order kinetic model in the terms of higher correlation coefficients (R^2) and lower SSE values. Furthermore, a striking similarity between the experimental/ calculated q_e values symbolize anions adsorption is explained well by Pseudo-second-order model in preference to other models.

6.8 Adsorption Dynamics

Thermodynamic parameters, favouring the chelation of anionic species by TVFH were calculated from Van't Hoff plot (fig 6.16) and tabulated in table 6.13, negative free energy values registers, spontaneous and feasible sorption process. Also, positive values of standard enthalpy/entropy prove, the nature of the systems to be endothermic i.e., promoting increased affinity of anions and with greater degree of freedom at solid – liquid interface during elevated temperatures[18]. Similar behaviour was reported in the sorption of anions using modified rice husk[19].

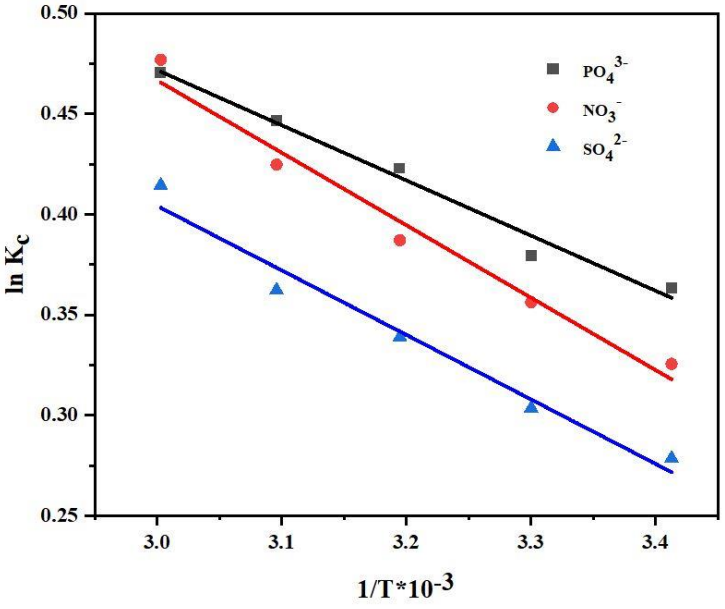

Figure 6.16 Van't Hoff Plot

Table 6.13 Thermodynamic Constants

Temp. (K)	PO_4^{3-} - TVFH			NO_3^--TVFH			SO_4^{2-} -TVFH		
	$\Delta G°x10^{-3}$ kJ/ mol	$\Delta H°$ kJ/mol	$\Delta S°$ kJ/mol	$\Delta G°x10^{-3}$ kJ/ mol	$\Delta H°$ kJ/mol	$\Delta S°$ kJ/mol	$\Delta G°x10^{-3}$ kJ/mol	$\Delta H°$ kJ/mol	$\Delta S°$ kJ/ mol
293	-0.88	2.28	10.76	-0.79	2.99	12.86	-0.67	2.66	11.36
303	-0.95			-0.89			-0.76		
313	-1.10			-1.00			-0.88		
323	-1.19			-1.14			-0.97		
333	-1.30			-1.32			-1.14		

6.9 Refrences

[1] S L Goertzen, K. D Thériault, A. M Oickle, A. C Tarasuk and H.A Andreas, Standardization of the Boehm Titration—part I: CO_2 *Expulsion and Endpoint determination*, Carbon, 48(4) **(2010)** 1252–1261

[2] Gulsum Karacetin, Sezen Sivrikaya, Mustafa Imamo glu, Adsorption of methylene blue from aqueous solutions by activated carbon prepared from hazelnut husk using zinc chloride, *Journal of Analytical Application and Pyrolysis.*110 **(2014)** 270–276

[3] M. Jain, V. K. Garg and K. Kadirvelu, Cadmium (II) Sorption and Desorption in a Fixed Bed Column using Sunflower Waste Carbon Calcium-Alginate Beads, *Bioresource Technology,* 129 **(2013)** 242–248

[4] Vishal.R.Parate, Mohammed.I.Talib, Study of Metal Adsorbent Prepared from Tur Dal (*Cajanus cajan*) Husk: A Value Addition to Agro-waste, *IOSR Journal of Environmental Science, Toxicology and Food Technology,* 9(3) **(2014)** 43- 54

[5] VK Gupta and A Rastogi, Biosorption of lead from aqueous solutions by green algae Spirogyra species: Kinetics and equilibrium studies, *Journal of Hazardous Materials,* 152 **(2008)** 407-414

[5] Charles Emeka Osakwe, Isma'il Sanni, Suraj Sa'id and Adamu Zubairu, Adsorption of Heavy Metals from Wastewaters using *Adonosia digitata* Fruit Shells and *Theobroma cacao* Pods as Adsorbents: A Comparative Study, *AU Journal of Technology,* 18(1) **(2014)**11-18

[6] Ammar Touil & Moussa Amrani, Removal of Nitrate ($N\mathbf{O_3^-}$) from Aqueous Solution using Adsorbent from Agricultural Residues: Equilibrium and Kinetic Studies, *Séminaire International Hydrogéologie Environnement*, **(2013)** 593 - 600

[7] B.M.W.P.K. Amarasinghe, R.A. Williams, Tea Waste as a Low-cost Adsorbent for the Removal of Cu and Pb from Wastewater, *Chemical Engineering Journal,* 132 **(2007)** 299-309

[8] Alka Shukla, Yu-Hui Zhang, P. Dubey, J.L. Margrave, Shyam S. Shukla, The Role of Sawdust in the Removal of Unwanted Materials from Water, *Journal of Hazardous Materials,* 95 **(2002)** 137-152

[9] Z. Aksu, A.B. Akın, Comparison of Remazol Black B, Biosorptive properties of live and treated activated sludge, *Chemical Engineering Journal*, 165 **(2010)** 184–193

[10] M. Otero, F. Rozada, L.F. Calvo, A.I. Garcıa, A. Morán, Elimination of organic water pollutants using adsorbents obtained from sewage sludge, *Dyes Pigments,* 57 **(2003)** 55–65

[11] Manali Rathod, Kalpana Mody, Shaik Basha, Efficient removal of phosphate from aqueous solutions by red seaweed, *Kappaphycus alverezii*, *Journal of Cleaner Production,* XXX **(2014)** 1 -10

[12] Artis Robalds, Liga Dreijalte, Oskars Bikovens and Maris Klavins, A Novel Peat-based Biosorbent for the Removal of Phosphate from Synthetic and Real Wastewater and Possible Utilization of Spent Sorbent in Land Application, *Desalination and Water Treatment,* 57 **(2016)** 13285–13294

[13] Bayram Kizilkaya, and Adem TekJnay A. Utilization to Remove Pb (II) Ions from Aqueous Environments using Waste Fish Bones by Ion Exchange, *Journal of Chemistry,* **(2014)** 1-12

[14] Xianze Wang, Zhongmou Liu, Jiancong Liu, Mingxin Huo, Hongliang Hu and Wu Yang, Removing Phosphorus from Aqueous Solutions Using Lanthanum Modified Pine Needles, *PLOS ONE,* **(2015)** 1 - 16

[15] C. Namasivayam and d. Sangeetha, Removal and Recovery of nitrate from Water by $ZnCl_2$ Activated Carbon from Coconut Coir Pith, an Agricultural Solid Waste, *International Journal of Chemical Technology*, 12 **(2005)** 513 – 521

[16] Hakan Demiral, Gül Gündüzog˘lu, Removal of nitrate from aqueous solutions by activated carbon prepared from sugar beet bagasse, *Bioresource Technology*, 101 **(2010)** 1675 - 1680

[17] Cengeloglu, Y., Tor, A., Ersoz, M., Arslan, G., Removal of nitrate from aqueous solution by using red mud, *Separation Purification Technology*, 51 **(2006)** 374-378

[18] Anni Keranen, Tiina Leiviska, Osmo Hormi, Juha Tanskanen, Removal of nitrate by modified pine sawdust: Effects of temperature and co-existing anions, *Journal of Environmental Management,* 147 **(2015)** 46 -54

[19] P. S. Kumar, S. Ramalingam, S. D. Kirupha, A. Murugesan, T. Vidyadevii and S. Sivanesan, Adsorption Behaviour of Nickel (II) onto Cashew Nut Shell: Equilibrium, Thermodynamic, Mechanism and Process Design, *Chemical Engineering Journal*, 167 **(2011)** 122–131.